Modification of band structure by oxygen filling in epitaxial La_{0.88}Sr_{0.12}MnO_{3-x} thin films

Sangkyun Ryu^{1,‡}, Jaejin Hwang^{1,‡}, Jin H. Cho², Younghak Kim³, Ambrose Seo⁴, Jaekwang Lee^{1,*}, Hyoungjeen Jeen^{1,5,*}

KEYWORDS: manganite thin film, x-ray absorption spectroscopy, pulsed laser deposition, oxygen vacancy, band structure

ABSTRACT: Oxygen stoichiometry is a critical factor in transition metal oxides, such as manganites, as it has a substantial influence on their electronic and magnetic properties through the generation of oxygen vacancies. However, the significance of oxygen stoichiometry is often underestimated in manganite thin films. In this study, we explore the formation of oxygen vacancies within La_{0.88}Sr_{0.12}MnO₃ (LSMO) under standard thin film deposition conditions and elucidate how these vacancies can be effectively filled through exposure to high oxygen partial pressure (*P*O₂) on the order of several hundred Torr during the cooling phase. The oxygen replenishment process has a profound impact on the electronic band structure, resulting in alterations in the electron occupancy near the Fermi level. This phenomenon is observed by optical spectroscopy and analyzed by density functional theory calculations. These findings underscore the indispensable nature of post-deposition oxygen annealing steps to attain stoichiometric LSMO thin films.

INTRODUCTION

Oxygen vacancies in perovskite transition metal oxides (TMO's) are often considered as functional defects due to their involvement in electronic transport, indirect magnetic interactions, and ionic conduction.¹⁻⁴ Consequently, significant efforts have been dedicated to enhancing the processing conditions for the synthesis of TMO thin films. Some previous studies have focused on understanding the relationship between epitaxial strain and the formation of oxygen vacancies, as well as the dynamics of oxygen migration between substrates and oxide films. 5-8 In addition, several studies have explored the impact of oxygen partial pressure during the cooling process on the creation of oxygen vacancies⁹⁻¹¹ In contrast to other TMO's^{12, 13}, it is known that oxygen vacancies are not readily formed in manganese-based oxides under conventional synthesis conditions, such as oxygen partial pressures (PO2) and temperatures. 14, 15 In some cases, an excess of oxygen content can be problematic when attempting to create bulk-like manganite thin films. 16-¹⁸ While numerous studies have been conducted on the influence of oxygen vacancy concentration on electrical and magnetic properties, 19-21 fewer studies have focused on the modification of the band structure by oxygen vacancies. In this regard, it is crucial to address how to replenish oxygen vacancies and what effect the oxygen filling has on the band structure.

To address this question, we selected lightly hole-doped $La_{0.88}Sr_{0.12}MnO_{3-x}$ (LSMO) as our model system. In the phase diagram with respect to hole doping²², even slight changes in the La/Sr ratio result in significant changes in electronic and magnetic properties. Since the formation of oxygen vacancies also affects the Mn valence state, it may also lead to substantial changes in physical properties.

In this study, we investigate the formation and removal of oxygen vacancies in La_{0.88}Sr_{0.12}MnO₃ under typical thin film processing conditions and their impact on the band structure and physical properties. In general, different *P*O₂ levels during the deposition process are used to control oxygen stoichiometry in oxide thin films.²³⁻²⁶ However, the pulsed laser deposition (PLD) process at different *P*O₂ levels can induce both cation and anion non-stoichiometry.^{24, 27, 28} To avoid this non-stoichiometric deposition during LSMO film growth, we have kept the same deposition conditions during the deposition and adjusted only the cooling *P*O₂ from 100 mTorr to 100, 300, and 500 Torr following the deposition. We demonstrate that not only the deposition *P*O₂ is an important parameter but also that the cooling *P*O₂ is critical for oxygen stoichiometry.

EXPERIMENTAL METHOD

For growing epitaxial LSMO thin films, a La_{0.88}Sr_{0.12}MnO₃ tar-TOSHIMA, from Japan and (LaAlO₃)_{0.3}(SrAl_{0.5}Ta_{0.5}O₃)_{0.7} (LSAT) substrates were used. Based on the lattice constants, it is expected that LSMO is in -1.24% of compressive strain by LSAT.²⁹ Growth is processed by pulsed laser deposition (PLD, Q-switched pulsed Nd:YAG laser with $\lambda = 355$ nm) with 0.9 J/cm² fluence. During LSMO thin film growth, the PO₂ was kept to 100 mTorr and the substrate temperature was 650 °C. After growth, different cooling PO₂ were used like 0.1 Torr, 100 Torr, 300 Torr, and 500 Torr. X-ray diffractometer (D8-discover, Bruker) was used for structural characterization. The θ -2 θ scan shows the out of plane lattice constant of LSMO thin films. For the strain state of LSMO thin films, X-ray reciprocal space mapping was collected. The temperature-dependent resistivity

¹Department of Physics, Pusan National University, Busan 46241, Korea

²Department of Physics Education, Pusan National University, Busan 46241, Korea

³Pohang Accelerator Laboratory, POSTECH, Pohang 37673, Korea

⁴Department of Physics and Astronomy, University of Kentucky, Lexington, KY 40506, USA

⁵Research Center for Dielectric and Advanced Matter Physics, Pusan National University, Busan 46241, Korea

measurements were performed. Also, the optical conductivity spectra of LSMO thin films were obtained using a spectroscopic ellipsometer (VASE, J. A. Woollam) with 65°, 70°, and 75° incident angles. To check the Mn valence state, x-ray absorption spectroscopy (XAS) was carried out in the 2A beamline of Pohang Accelerator Laboratory. The Mn L-edge and O K-edge were collected by total electron yield mode with normal incident angle at room temperature. Density functional theory (DFT) calculations were carried out to optimize La_{0.875}Sr_{0.125}MnO₃ and La_{0.875}Sr_{0.125}MnO₃ with oxygen vacancy (V₀) using the projector augmented wave (PAW) method with the plane-wave based Vienna Ab Initio Package (VASP).30-32 We used the spin-polarized generalized-gradient approximation (GGA) with the Perdew-Burke-Ernzerhof (PBE) functional for the exchange correlation functional.³³ We applied an effective Hubbard parameter $U_{\text{eff}} = U - J$ with 4 eV to localized Mn 3d orbitals. In all calculations, ferromagnetic (FM) collinear spin ordering is considered on the Mn ions. To describe the accurate electronic structures of La_{0.875}Sr_{0.125}MnO₃, we used hybrid Hartree-Fock (HF) - DFT method with the Heyd-Scuseria-Ernzerhof (HSE06) screened hybrid functional. ³⁴⁻³⁶ Γ-centered 4×4×4 k-point meshes were used for the electronic structure calculations of La_{0.875}Sr_{0.125}MnO₃. The calculations were converged in energy to 10⁻⁵ eV/cell and the structures were relaxed until the forces were less than 0.01 eV/Å.

RESULTS AND DISSCUSSION

To check the structural characteristics of these LSMO thin films cooled with different PO2, lattice constants were measured using X-ray diffraction. As shown in Figure 1 (a), four LSMO thin films show clear kiessig fringes around (001) and (002) LSMO peaks. The (002) LSMO peak is shifted to a higher angle as increasing the cooling PO₂. This peak shift indicates that the out of plane lattice constant of LSMO decreases with the increased cooling PO₂. Since oxygen vacancy formation in perovskite-based TMO thin films often result in the expansion of lattice, 8 this observation is likely to indicate the reduction of oxygen vacancies. Figures 1 (b) – (e) show X-ray reciprocal space maps displaying the in-plane and out-ofplane lattice constants of LSMO thin films with different cooling PO₂. The in-plane lattice constants of all LSMO thin films are close to that of LSAT, meaning that the in-plane lattice constant of LSMO thin films is coherently strained to LSAT substrates with successful epitaxial growth. The out-of-plane lattice constants are 3.94 Å for the film cooled at 0.1 Torr of PO_2 , 3.94 Å for the film cooled at 100 Torr, 3.93 Å for the film cooled at 300 Torr, and 3.92 Å for the film cooled at 500 Torr. This is consistent with the results from the θ -2 θ scans. Note that the bulk lattice constants of LSMO are a = b = 3.916 Å and c = 3.892 Å in a tetragonal structure.³⁷ The slightly larger lattice constant in our thin films is due to the compressive strain by LSAT substrates (a = 3.868 Å, cubic) with -1.24% lattice mismatch.²⁹ Besides elastic deformation, stoichiometric factors, such as oxygen vacancies and cation stoichiometry, play a critical role in inelastic deformation mechanisms that lead to variations in lattice constants.³⁸⁻⁴⁰ It has been reported that the modification of cation stoichiometry is highly susceptible to the deposition parameters such as gas pressures, laser fluence, and temperature, due to the complex confluence from laser plume and the plume-substrate interface. 23-25, 27, 41, 42 However, such changes primarily occur during the deposition process. Another possible reason for variations in lattice constants arises during the cooling process.³⁹ Differences in the oxygen chemical potential between the deposition and cooling processes often manifest as the changes in lattice constants, which are often observed in other oxides such as NdNiO₃, LaMnO₃ and SrTiO₃. 43-45 Since we specifically manipulated the cooling PO2, the observed change in lattice constants is likely due to the elimination of oxygen vacancies.

The change in electronic transport depending on the cooling PO₂ of LSMO thin films was investigated. Figure 2 (a) shows the temperature-dependent resistivity of LSMO thin films. At the 0.1 Torr of cooling PO2, the LSMO thin film behaves like a typical insulator. In contrast, slight changes in the slope are seen at around 150 K from the LSMO thin films with 100 Torr of cooling PO₂. In thease of the LSMO thin films cooled at 300 Torr and 500 Torr of PO₂, a clear insulator-to-metal transition is seen from each film as shown in the insets of Figure 2 (a). The transition temperatures (T_{IM}) of LSMO thin films cooled at 300 Torr and 500 Torr of PO₂ are 187 K and 190 K, respectively. The $T_{\rm IM}$ of the LSMO thin films is increased as the cooling PO_2 is increased. Note that the T_{IM} of bulk LSMO is 172 K.46 In addition, The LSMO thin films cooled at 300 Torr and 500 Torr of PO2 undergo another transition by increase of resistivity at around 165 K. The metal to insulator transition is attributed to the appearance of orbital ordering as seen in the bulk LSMO (x = 0.12). 46,47 These results show that the LSMO films cooled at 300 Torr and 500 Torr of PO2 exhibit electrical properties similar to bulk material LSMO (x = 0.12). In the case of LSMO thin films at 0.1 Torr and 100 Torr of PO2, the insulator to metal transition is not clearly observed. The poor phase transition is reported by S. Kumari, et al., due to oxygen vacancy.³⁹

As shown in Figure 2 (b), optical conductivity as a function of photon energy was extracted from spectroscopic ellipsometry. As shown in Figure 2 (b), we proceed the deconvolution of the optical conductivity results using multiple Lorentzian as shown as Table 1. We found the two peaks as A and B(dot line) from the *d-d* transition at Mn. 48-50 The peak A of LSMO thin film cooled at 0.1Torr of PO2 is located at the lower energy compared to those of LSMO thin films cooled at 100, 300, and 500 Torr of PO2. The peak shift in peak A means that electrons in the valence band of LSMO can transit across the Fermi level with the lower energy. 48, 51, 52 The oxygen vacancies in LSMO were filled by the addition of oxygen, leading to a reduction in the valence state electrons of Mn, electrons are removed from the band associated with the transition of the A peak, its position is shifted to higher energy. The B peak is situated at a higher energy level compared to peak A, indicating the presence of electron removal due to oxygen addition in the band correlated with peak A. Our optical conductivity results show this change in the electronic structure. As shown as Table. 1, the A peak position of LSMO cooled at 0.1 Torr of PO2, is 0.88 eV. However, upon oxygen filling, the A peak position of LSMO cooled at 100 Torr of PO₂, is 1.04 eV as shown in Figure 2 (c). The cooling PO₂ affects the number of electrons in the valence band. The modification of electronic structure may be inferred from optical conductivity results.

To theoretically reveal the electronic structure change under different PO2 conditions (0.1 Torr and 500 Torr), two crystal structures of La_{0.875}Sr_{0.125}MnO₃ with one V_o (Figure 3 (a)) and La_{0.875}Sr_{0.125}MnO₃ without V_o (Figure 3 (b)) were considered in our DFT calculations. Here, La_{0.875}Sr_{0.125}MnO₃ w/ V_o represents the LSMO thin film with 0.1 Torr of cooling PO₂ corresponding to the oxygen deficient LSMO_{3-x} structure. In contrast, La_{0.875}Sr_{0.125}MnO₃ w/o V_o corresponds to the stoichiometric LSMO thin film with 500 Torr of cooling PO₂. Figure 3 (a) and (b) show the density of states (DOS) of La_{0.875}Sr_{0.125}MnO₃ w/ V_o (upper panel) and La_{0.875}Sr_{0.125}MnO₃ w/o V_o (lower panel), respectively. Here, we aligned the O 1s level of the La_{0.875}Sr_{0.125}MnO₃ w/V_o structure with the O 1s level of La_{0.875}Sr_{0.125}MnO₃ w/o Vo structure to directly compare the Fermi levels of two structures, and find that the fermi level of La_{0.875}Sr_{0.125}MnO₃ w/ V_o is approximately 0.46 eV higher than that of the $La_{0.875}Sr_{0.125}MnO_3\,w/o\,\,V_o$ structure. In addition, we find that the band gap of La_{0.875}Sr_{0.125}MnO₃ w/ V_o representing LSMO thin film with 0.1 Torr of cooling PO₂ is lowered by about 0.4 eV due to the oxygen vacancy compared with that of $La_{0.875}Sr_{0.125}MnO_3$ w/o V_o corresponding stoichiometric LSMO thin film with 500 Torr of cooling PO_2 , which is consistent with the experimental observation of d-d transition lowering.

To check the different chemical information depending on cooling PO₂, the Mn L-edge and O K-edge were measured by x-ray absorption spectroscopy.^{53, 54} As shown in Figures 4 (a) and (b), the XAS spectra were collected at room temperature. The L_3 -edge is shifted by cooling PO_2 . The L_3 peak position of LSMO thin films with 0.1 Torr of cooling PO_2 is 644.05 eV, and the peak position is shifted to 644.15 eV by increasement of cooling PO2 as shown in Figure 4. This energy shift at the L_3 edge is well known means that the valence state of Mn is increased. 54-56 From this result, the cooling PO2 possibly affects Mn valence state of LSMO thin films. There are two possible ways to affect Mn valence state. The one is cation ratio change, but cation ratio change is hard to occur due to same deposition condition. The other is oxygen content. During the cooling process, 0.1 Torr of cooling PO₂ creates oxygen vacancies in lattice of LMSO thin films. The O K-edge is collected for metaloxygen hybridization, as shown in Figure 4 (b). In O K-edge spectra, the pre-peaks at around 532 eV is associated with Mn-O hybridization, which may be affected by PO2.54 As shown in the inset of Figure 4, the integration of pre-peak is increased depending on cooling PO2. In similar system as La_{0.7}Sr_{0.3}MnO₃, N. Wang, et al. reported that this decrease in the intensity of the pre-peak was evidence of the generation of oxygen vacancies.⁵⁷ In our case, this increment in pre-peak intensity by the increase of cooling PO2 means that the LSMO thin film cooled at 0.1 Torr of PO2 contains more oxygen vacancies compare to those in LSMO thin films cooled at 100, 300, and 500 Torr of PO2.58

CONCLUSIONS

In conclusion, oxygen-stoichiometric manganite thin films can be obtained by increasing PO_2 to a few hundred Torr during cooling following deposition. To reduce the number of oxygen vacancies, it is required to cool the oxides in high oxygen partial pressures. In this work, we used lightly hole-doped LSMO thin films, and the LSMO thin film cooled in 0.1 Torr of PO_2 includes noticeable amount of oxygen vacancies. The oxygen filling is clearly seen at the LSMO thin films cooled at 300 Torr or higher from structural, optical spectroscopy, and x-ray absorption spectroscopy. The LSMO thin film cooled at the higher PO_2 shows reduction of lattice constant, associated increase of optical transition energy backed by theoretical calculation, and increase of metal-oxygen hybridization. These changes in physical properties were helpful to understand the synthesis of complex oxides.

AUTHOR INFORMATION

Corresponding Author

Jackwang Lee - Department of Physics, Pusan National University, Busan 46241, Korea

email: jaekwangl@pusan.ac.kr

Hyoungjeen Jeen - Department of Physics, Pusan National University, Busan 46241, Korea email: hjeen@pusan.ac.kr

Authors

Sangkyun Ryu - Department of Physics, Pusan National University, Busan 46241, Korea

Jaejin Hwang - Department of Physics, Pusan National University, Busan 46241, Korea

Jin H. Cho - Department of Physics Education, Pusan National University, Busan 46241, Korea

Younghak Kim - Pohang Accelerator Laboratory, POSTECH, Pohang 37673, Korea

Ambrose Seo - Department of Physics and Astronomy, University of Kentucky, Lexington, Kentucky 40506, USA

Author Contributions

‡These authors contributed equally.

ACKNOWLEDGMENT

This research was supported by NRF-Korea (NRF-2018R1D1A1B07045462). J. L. and H. J. acknowledge the support of the Korea Basic Science Institute (National Research Facilities and Equipment Center) through a grant funded by the Ministry of Education (no. 2021R1A6C101A429) for spectroscopic ellipsometry, x-ray diffraction, and DFT calculation. A. S. was supported by National Science Foundation (Grant No. DMR-2104296). S. R. was supported by PNU-RENovation(2021-2022).

REFERENCES

- (1) Kalinin, S. V.; Borisevich, A.; Fong, D. Beyond condensed matter physics on the nanoscale: the role of ionic and electrochemical phenomena in the physical functionalities of oxide materials. ACS nano 2012, 6 (12), 10423-10437.
- (2) Kalinin, S. V.; Spaldin, N. A. Functional ion defects in transition metal oxides. *Science* **2013**, *341* (6148), 858-859. (3) Goodenough, J. B. Theory of the role of covalence in the perovskite type manganites [La,M(II)]MnO₃. *Phys. Rev.* **1955**, *100* (2), 564-573.
- (4) Maier, J. Nanoionics: ion transport and electrochemical storage in confined systems. *Nat. Mater* **2005**, *4*, 805-815.
- (5) Petrie, J. R.; Mitra, C.; Jeen, H.; Choi, W. S.; Meyer, T. L.; Reboredo, F. A.; Freeland, J. W.; Eres, G.; Lee, H. N. Strain control of oxygen vacancies in epitaxial strontium cobaltite films. *Adv. Funct. Mater.* **2016**, *26* (10), 1564-1570.
- (6) Kang, K. T.; Zhang, B.; Sharma, Y.; Paudel, B.; Wang, H.; Dowden, P.; Chen, A. Substrate oxygen sponge effect: A parameter for epitaxial manganite thin film growth. *Appl. Phys. Lett.* **2020**, *117* (15).
- (7) Corey, Z.; Han, H. H.; Kang, K. T.; Wang, X.; Lalk, R. A.; Paudel, B.; Roy, P.; Sharma, Y.; Yoo, J.; Jia, Q. The Role of Oxygen Transfer in Oxide Heterostructures on Functional Properties. *Adv. Mater. Interfaces* **2022**, *9* (11), 2101867.
- (8) Wang, L.; Yang, Z.; Wu, J.; Bowden, M. E.; Yang, W.; Qiao, A.; Du, Y. Time-and strain-dependent nanoscale structural degradation in phase change epitaxial strontium ferrite films. npj Mater. Degrad. 2020, 4 (1), 16.
- (9) Gao, R.; Yang, H.; Chen, Y.; Sun, J.; Zhao, Y.; Shen, B. Effect of cooling oxygen pressure on the photoconductivity in Bi0. 9La0. 1FeO3 thin films. *J. Alloys Compd* **2014**, *591*, 346-350
- (10) Jeen, H.; Choi, W. S.; Freeland, J. W.; Ohta, H.; Jung, C. U.; Lee, H. N. Topotactic phase transformation of the brownmillerite SrCoO_{2.5} to the perovskite SrCoO_{3-δ}. *Adv. Mater* **2013**, *25* (27), 3651-3656.
- (11) Khare, A.; Shin, D.; Yoo, T. S.; Kim, M.; Kang, T. D.; Lee, J.; Roh, S.; Jung, I. H.; Hwang, J.; Kim, S. W. Topotactic metal-insulator transition in epitaxial SrFeOx thin films. *Adv. Mater* **2017**, *29* (37), 1606566.
- (12) Choi, W. S.; Jeen, H.; Lee, J. H.; Seo, S. A.; Cooper, V. R.; Rabe, K. M.; Lee, H. N. Reversal of the lattice structure in SrCoO_x epitaxial thin films studied by real-time optical spectroscopy and first-principles calculations. *Phys. Rev. Lett.* 2013, 111 (9), 097401.
- (13) Jeen, H.; Choi, W. S.; Biegalski, M. D.; Folkman, C. M.; Tung, I. C.; Fong, D. D.; Freeland, J. W.; Shin, D.; Ohta, H.; Chisholm, M. F.; Lee, H. N. Reversible redox reactions in an epitaxially stabilized SrCoO_x oxygen sponge. *Nat. Mater* **2013**, *12* (11), 1057-1063.

- (14) Kuo, J. H.; Anderson, H. U.; Sparlin, D. M. Oxidation-reduction behavior of undoped and Sr-doped LaMnO₃ nonstoichiometry and defect structure. *J. Solid State Chem.* **1989**, 83 (1), 52-60.
- (15) Mizusaki, J.; Mima, Y.; Yamauchi, S.; Fueki, K.; Tagawa, H. Nonstoichiometry of the perovskite-type oxides La_{1-x}Sr_xCoO_{3-δ}. *J. Solid State Chem.* **1989**, *80* (1), 102-111. (16) Choi, W. S.; Marton, Z.; Jang, S. Y.; Moon, S. J.; Jeon, B. C.; Shin, J. H.; Seo, S. S. A.; Noh, T. W.; Myung-Whun, K.; Lee, H. N.; Lee, Y. S. Effects of oxygen-reducing aTMO'sphere annealing on LaMnO₃ epitaxial thin films. *J. Phys. D: Appl. Phys.* **2009**, *42* (16), 165401.
- (17) Marton, Z.; A. Seo, S. S.; Egami, T.; Lee, H. N. Growth control of stoichiometry in LaMnO₃ epitaxial thin films by pulsed laser deposition. *J. Cryst. Growth* **2010**, *312* (20), 2923-2927. (18) Suntivich, J.; May, K. J.; Gasteiger, H. A.; Goodenough, J. B.; Shao-Horn, Y. A perovskite oxide optimized for oxygen evolution catalysis from molecular orbital principles. *Science* **2011**, *334* (6061), 1383-1385.
- (19) Rasic, D.; Sachan, R.; Temizer, N. K.; Prater, J.; Narayan, J. Oxygen effect on the properties of epitaxial (110) La_{0.7}Sr_{0.3}MnO₃ by defect engineering. *ACS Appl. Mater. Interfaces* **2018**, *10* (24), 21001-21008.
- (20) Yao, L.; Inkinen, S.; Van Dijken, S. Direct observation of oxygen vacancy-driven structural and resistive phase transitions in La_{2/3}Sr_{1/3}MnO₃. *Nat Commun* **2017**, 8 (1), 14544.
- (21) Cao, L.; Petracic, O.; Zakalek, P.; Weber, A.; Rücker, U.; Schubert, J.; Koutsioubas, A.; Mattauch, S.; Brückel, T. Reversible Control of Physical Properties via an Oxygen-Vacancy-Driven Topotactic Transition in Epitaxial La_{0.7}Sr_{0.3}MnO₃₋₈ Thin Films. *Adv. Mater* **2019**, *31* (7), 1806183. (22) Urushibara, A.; Moritomo, Y.; Arima, T.; Asamitsu, A.; Kido, G.; Tokura, Y. Insulator-metal transition and giant magnetoresistance in La_{1-x}Sr_xMnO₃. *Phys. Rev. B* **1995**, *51* (20), 14103-14109.
- (23) Orgiani, P.; Ciancio, R.; Galdi, A.; Amoruso, S.; Maritato, L. Physical properties of La_{0.7}Ba_{0.3}MnO_{3-delta} complex oxide thin films grown by pulsed laser deposition technique. *Appl. Phys. Lett.* **2010**, *96* (3), 032501.
- (24) Wicklein, S.; Sambri, A.; Amoruso, S.; Wang, X.; Bruzzese, R.; Koehl, A.; Dittmann, R. Pulsed laser ablation of complex oxides: The role of congruent ablation and preferential scattering for the film stoichiometry. *Appl. Phys. Lett.* **2012**, *101* (13), 5. (25) Chen, J.; Döbeli, M.; Stender, D.; Conder, K.; Wokaun, A.; Schneider, C. W.; Lippert, T. Plasma interactions determine the composition in pulsed laser deposited thin films. *Appl. Phys. Lett.* **2014**, *105* (11), 114104.
- (26) Lee, H. N.; Ambrose Seo, S. S.; Choi, W. S.; Rouleau, C. M. Growth control of oxygen stoichiometry in homoepitaxial SrTiO₃ films by pulsed laser epitaxy in high vacuum. *Sci. Rep.* **2016**, *6*, 19941.
- (27) Shimamoto, K.; Dobeli, M.; Lippert, T.; Schneider, C. W. Cation ratio and ferroelectric properties of TbMnO₃ epitaxial films grown by pulsed laser deposition. *J. Appl. Phys.* **2016**, *119* (18), 5.
- (28) Lee, S. A.; Jeong, H.; Woo, S.; Hwang, J. Y.; Choi, S. Y.; Kim, S. D.; Choi, M.; Roh, S.; Yu, H.; Hwang, J. Phase transitions via selective elemental vacancy engineering in complex oxide thin films. *Sci. Rep.* 2016, 6 (1), 1-10. (29) Kim, Y.; Ryu, S.; Jeen, H. Strain-effected physical properties of ferromagnetic insulating La_{0.88}Sr_{0.12}MnO₃ thin films. *RSC Adv.* 2019, 9 (5), 2645-2649.
- (30) Blöchl, P. E. Projector augmented-wave method. *Phys. Rev. B* **1994**, *50* (24), 17953.
 - (31) Kresse, G.; Hafner, J. Ab initio molecular dynamics for liquid metals. *Phys. Rev. B* **1993**, *47* (1), 558.

- (32) Kresse, G.; Furthmüller, J. Efficient iterative schemes for ab initio total-energy calculations using a plane-wave basis set. *Phys. Rev. B* **1996**, *54* (16), 11169.
- (33) Perdew, J. P.; Ruzsinszky, A.; Csonka, G. I.; Vydrov, O. A.; Scuseria, G. E.; Constantin, L. A.; Zhou, X.; Burke, K. Restoring the density-gradient expansion for exchange in solids and surfaces. *Phys. Rev. Lett.* **2008**, *100* (13), 136406.
- (34) Heyd, J.; Scuseria, G. E.; Ernzerhof, M. Hybrid functionals based on a screened Coulomb potential. *J. Chem. Phys.* **2003**, *118* (18), 8207-8215.
- (35) Paier, J.; Marsman, M.; Hummer, K.; Kresse, G.; Gerber, I.
 C.; Ángyán, J. G. Screened hybrid density functionals applied to solids. *J. Chem. Phys.* 2006, 124 (15).
- (36) Heyd, J.; Scuseria, G. E.; Ernzerhof, M. Erratum: "Hybrid functionals based on a screened Coulomb potential" [J. Chem. Phys. 118, 8207 (2003)]. *J. Chem. Phys.* **2006**, *124* (21). (37) Cox, D. E.; Iglesias, T.; Moshopoulou, E.; Hirota, K.; Takahashi, K.; Endoh, Y. Vertical boundary at x ~ 0.11 in the structural phase diagram of the La_{1-x}Sr_xMnO₃ system (0.08 ≤ x ≤
- 0.125). *Phys. Rev. B* **2001**, *64* (2), 024431. (38) Koohfar, S.; Disa, A. S.; Marshall, M. S. J.; Walker, F. J.; Ahn, C. H.; Kumah, D. P. Structural distortions at polar
- manganite interfaces. *Phys. Rev. B* **2017**, *96* (2), 024108. (39) Kumari, S.; Mottaghi, N.; Huang, C. Y.; Trappen, R.; Bhandari, G.; Yousefi, S.; Cabrera, G.; Seehra, M. S.; Holcomb, M. B. Effects of oxygen modification on the structural and magnetic properties of highly epitaxial La_{0.7}Sr_{0.3}MnO₃ (LSMO) thin films. *Sci. Rep.* **2020**, *10* (1), 1-11.
- (40) Mazza, A. R.; Lu, Q. Y.; Hu, G. X.; Li, H. X.; Browning, J. F.; Charlton, T. R.; Brahlek, M.; Ganesh, P.; Ward, T. Z.; Lee, H. N. Reversible Hydrogen-Induced Phase Transformations in La_{0.7}Sr_{0.3}MnO₃ Thin Films Characterized by In Situ Neutron Reflectometry. *ACS Appl. Mater. Interfaces* **2022**, *14* (8), 10898-10906
- (41) Lee, S. A.; Jeong, H.; Woo, S.; Hwang, J. Y.; Choi, S. Y.; Kim, S. D.; Choi, M.; Roh, S.; Yu, H.; Hwang, J. Phase transitions via selective elemental vacancy engineering in complex oxide thin films. *Sci. Rep.* **2016**, *6*, 23649.
- (42) Chen, A.; Su, Q.; Han, H.; Enriquez, E.; Jia, Q. Metal oxide nanocomposites: a perspective from strain, defect, and interface. *Adv. Mater* **2019**, *31* (4), 1803241.
- (43) Tyunina, M.; Rusevich, L.; Kotomin, E. A.; Pacherova, O.; Kocourek, T.; Dejneka, A. Epitaxial growth of perovskite oxide films facilitated by oxygen vacancies. *J. Mater. Chem. C* **2021**, *9* (5), 1693-1700.
- (44) Miyoshi, S.; Hong, J. O.; Yashiro, K.; Kaimai, A.; Nigara, Y.; Kawamura, K.; Kawada, T.; Mizusaki, J. Lattice expansion upon reduction of perovskite-type LaMnO₃ with oxygen-deficit nonstoichiometry. *Solid State Ion.* 2003, 161 (3-4), 209-217.
 (45) Tyunina, M.; Pacherova, O.; Kocourek, T.; Dejneka, A. Anisotropic chemical expansion due to oxygen vacancies in perovskite films. *Sci. Rep.* 2021, 11 (1), 1-6.
- (46) Endoh, Y.; Hirota, K.; Ishihara, S.; Okamoto, S.; Murakami, Y.; Nishizawa, A.; Fukuda, T.; Kimura, H.; Nojiri, H.; Kaneko, K. Transition between two ferromagnetic states driven by orbital ordering in La_{0.88}Sr_{0.12}MnO₃. *Phys. Rev. Lett.* **1999**, *82* (21), 4328. (47) Nojiri, H.; Kaneko, K.; Motokawa, M.; Hirota, K.; Endoh,
- Y.; Takahashi, K. Two ferromagnetic phases in La_{1-x}Sr_xMnO₃ (x~ 1/8). *Phys. Rev. B* **1999**, *60* (6), 4142.
- (48) Takenaka, K.; Sawaki, Y.; Shiozaki, R.; Sugai, S. Electronic structure of the double-exchange ferromagnet La_{0.825}Sr_{0.175}MnO₃ studied by optical reflectivity. *Phys. Rev. B* **2000**, *62* (21), 13864. (49) Lee, H. J.; Jung, J. H.; Lee, Y. S.; Ahn, J. S.; Noh, T. W.; Kim, K. H.; Cheong, S. W. Optical properties of a Nd_{0.7}Sr_{0.3}MnO₃ single crystal. *Phys. Rev. B* **1999**, *60* (8), 5251.

- (50) Quijada, M.; Černe, J.; Simpson, J.; Drew, H.; Ahn, K.; Millis, A.; Shreekala, R.; Ramesh, R.; Rajeswari, M.; Venkatesan, T. Optical conductivity of manganites: Crossover from Jahn-Teller small polaron to coherent transport in the ferromagnetic state. *Phys. Rev. B* 1998, 58 (24), 16093.
- (51) Kim, J.; Shrestha, S.; Souri, M.; Connell, J. G.; Park, S.; Seo, A. High-temperature optical properties of indium tin oxide thin-films. *Sci. Rep.* **2020**, *10* (1), 12486.
- (52) Turky, A. O.; Rashad, M. M.; Hassan, A. M.; Elnaggar, E. M.; Bechelany, M. Optical, electrical and magnetic properties of lanthanum strontium manganite La_{1-x}Sr_xMnO₃ synthesized through the citrate combustion method. *Phys. Chem. Chem. Phys.* 2017, 19 (9), 6878-6886.
- (53) Kang, J. S.; Kim, J. H.; Sekiyama, A.; Kasai, S.; Suga, S.; Han, S. W.; Kim, K. H.; Muro, T.; Saitoh, Y.; Hwang, C.; Olson, C. G.; Park, B. J.; Lee, B. W.; Shim, J. H.; Park, J. H.; Min, B. I. Bulk-sensitive photoemission spectroscopy of A2FeMoO6 double perovskites (A=Sr, Ba). *Phys. Rev. B* **2002**, *66* (11), 113105. (54) Abbate, M.; de Groot, F. M. F.; Fuggle, J. C.; Fujimori, A.; Strebel, O.; Lopez, F.; Domke, M.; Kaindl, G.; Sawatzky, G. A.; Takano, M.; Takeda, Y.; Eisaki, H.; Uchida, S. Controlled-valence properties of La_{1-x}Sr_xFeO₃ and La_{1-x}Sr_xMnO₃ studied by

- soft-x-ray absorption spectroscopy. *Phys. Rev. B* **1992**, *46* (8), 4511-4519.
- (55) Sarma, D. D.; Rader, O.; Kachel, T.; Chainani, A.; Mathew, M.; Holldack, K.; Gudat, W.; Eberhardt, W. Contrasting behavior of homovalent-substituted and hole-doped systems: O *K*-edge spectra from LaNi_{1-x}M_xO₃(M=Mn, Fe, and Co) and La_{1-x}Sr_xMnO₃. *Phys. Rev. B* **1994**, *49* (20), 14238-14243.
- (56) Mierwaldt, D.; Mildner, S.; Arrigo, R.; Knop-Gericke, A.; Franke, E.; Blumenstein, A.; Hoffmann, J.; Jooss, C. In Situ XANES/XPS Investigation of Doped Manganese Perovskite Catalysts. *Catal.* 2014, 4 (2), 129-145.
- (57) Wang, N.; Hinokuma, S.; Ina, T.; Toriumi, H.; Katayama, M.; Inada, Y.; Zhu, C. Y.; Habazaki, H.; Aoki, Y. Incorporation of bulk proton carriers in cubic perovskite manganite driven by interplays of oxygen and manganese redox. *Chem. Mater.* **2019**, 31 (20), 8383-8393.
- (58) Wang, D.; Liou, S. H.; He, P.; Sellmyer, D. J.; Hadjipanayis, G. C.; Zhang, Y. SmFe₁₂ and SmFe₁₂N_x films fabricated by sputtering. *J. Magn. Magn. Mater.* 1993, 124 (1), 62-68.

Table of Contents

Figure 1. (a)The θ -2 θ scan x-ray diffraction pattern of LSMO on LSAT depending on cooling PO_2 shows a diffraction pattern around (001) LSAT and (002) LSAT plane. The (001)LSMO peak and (002)LSMO peak position is shifted to higher angles depending on the increase in cooling PO_2 . The Reciprocal space mapping image show around (103) LSAT plane, (b) is LSMO thin film cooled at 0.1 Torr of PO_2 , (c) is LSMO thin film cooled at 100 Torr of PO_2 , (d) is LSMO thin film cooled at 300 Torr of PO_2 , and (e) is LSMO thin film cooled at 500 Torr of PO_2 . The out of plane lattice constant is decreased depending on the increase in cooling PO_2 .

Figure 2. (a) The resistivity depending temperature of LSMO thin films with different cooling PO_2 . The dashed line represents the instrument limit due to the high resistivity of LSMO. The LSMO thin films cooled at 300 and 500 Torr of PO_2 show the insulator to metal transition and metal to insulator transition. (b) The optical conductivity of LSMO was obtained by ellipsometry. (c)The electronic structure schematic of LSMO films indicated the d-d transition, with the Fermi level represented by a red line.

TABLE I. The peak parameter of peak A and B is obtained from ellipsometry result. The peak position in peak A of LSMO cooled at 0.1 Torr of PO₂ is low energy shift to 0.88 eV to compare that of LSMO cooled at 100 Torr of PO₂ as 1.04 eV. The peak B of LSMO thin films were not shifted by cooling PO₂.

Figure 3. DFT optimized structures and projected density of states of (a) La_{0.875}Sr_{0.125}MnO₃ with V_O and (b) La_{0.875}Sr_{0.125}MnO₃. We aligned the O 1s level of the La_{0.875}Sr_{0.125}MnO₃ structure with the O 1s level of La_{0.875}Sr_{0.125}MnO₃ with V_O structure on the same line (black dashed line) to compare the Fermi levels of two structures. Zero energy represents the Fermi level. Schematic DOS near Fermi level for La_{0.875}Sr_{0.125}MnO₃ with V_O and La_{0.875}Sr_{0.125}MnO₃ show the energy difference between two fermi level, and band gap.

Figure 4. (a) The Mn L-edge spectra and (b) O K-edge spectra of LSMO thin films were obtained through x-ray absorption spectroscopy at room temperature. The peak of the Mn L_3 -edge shifts to a higher energy with an increase in cooling PO_2 . (Inset) The integrated value of the peak of Mn 3d-O 2p hybridization peak intensity of LSMO films cooled at higher PO_2 shifts to a higher value.

TABLE I. The peak parameter of peak A and B is obtained from ellipsometry result. The peak position in peak A of LSMO cooled at 0.1 Torr of PO₂ is low energy shift to 0.88 eV to compare that of LSMO cooled at 100 Torr of PO₂ as 1.04 eV. The peak B of LSMO thin films were not shifted by cooling PO₂.

Cooling PO ₂ (Torr)	A			В		
	Peak position (eV)	FWHM (eV)	Area	Peak po- sition (eV)	FWHM (eV)	Area
0.1	0.88	0.99	272	1.6	0.99	634
100	1.04	0.92	471	1.67	0.77	300
300	1.03	0.87	428	1.62	0.75	327
500	1.07	0.77	311	1.66	0.61	199

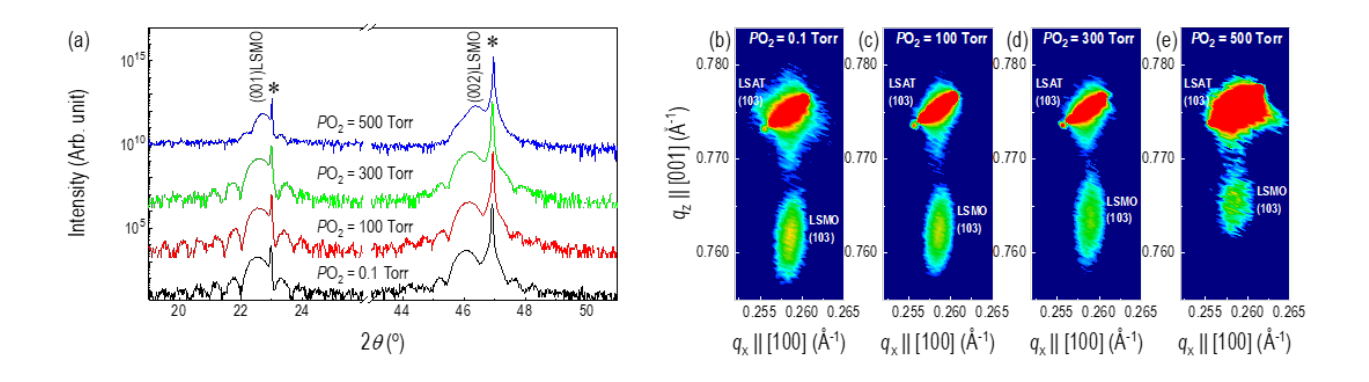


Figure 1. (a)The θ -2 θ scan x-ray diffraction pattern of LSMO on LSAT depending on cooling PO_2 shows a diffraction pattern around (001) LSAT and (002) LSAT plane. The (001)LSMO peak and (002)LSMO peak position is shifted to higher angles depending on the increase in cooling PO_2 . The Reciprocal space mapping image show around (103) LSAT plane, (b) is LSMO thin film cooled at 0.1 Torr of PO_2 , (c) is LSMO thin film cooled at 100 Torr of PO_2 , (d) is LSMO thin film cooled at 300 Torr of PO_2 , and (e) is LSMO thin film cooled at 500 Torr of PO_2 . The out of plane lattice constant is decreased depending on the increase in cooling PO_2 .

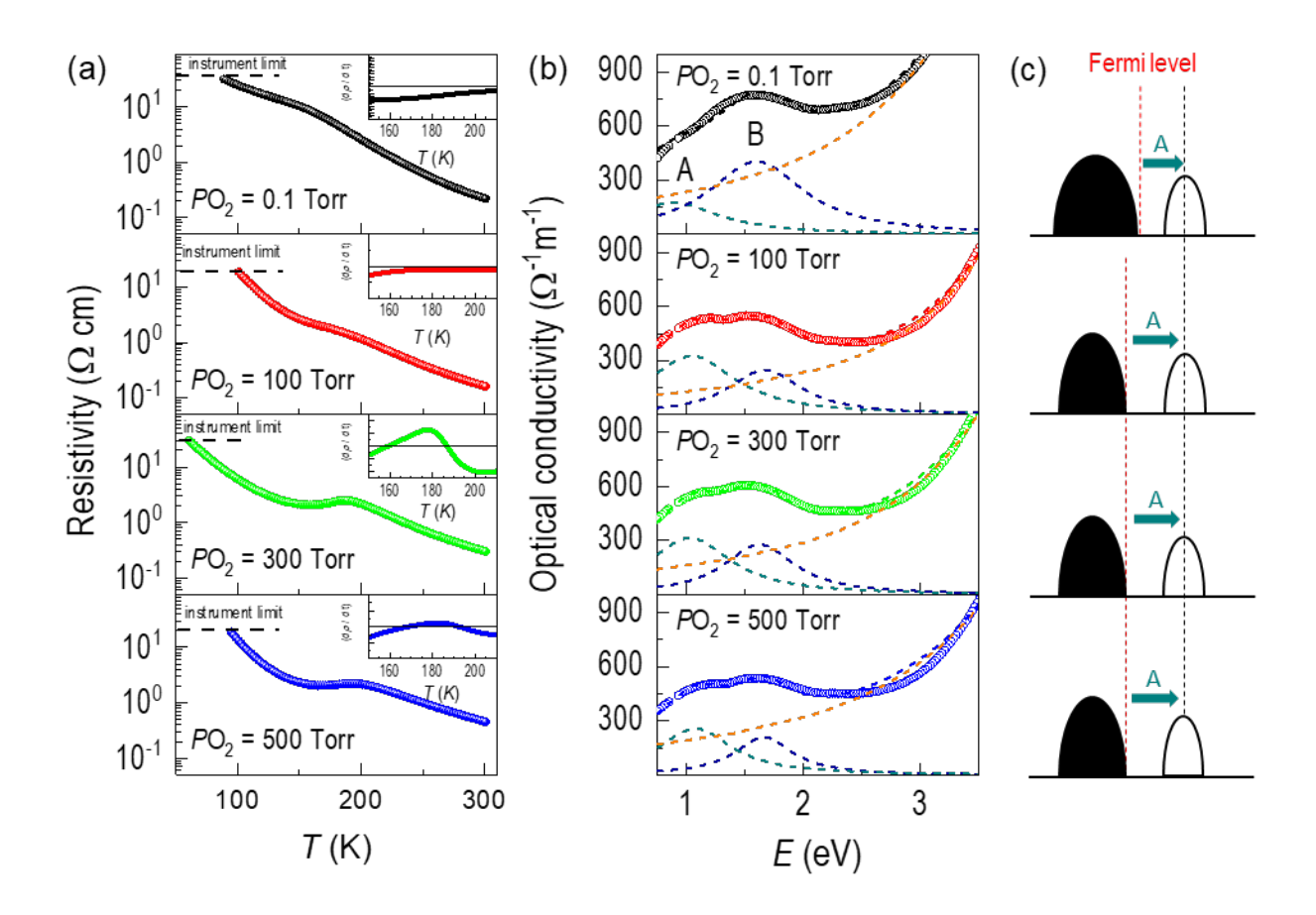


Figure 2. (a) The resistivity depending temperature of LSMO thin films with different cooling PO_2 . The dashed line represents the instrument limit due to the high resistivity of LSMO. The LSMO thin films cooled at 300 and 500 Torr of PO_2 show the insulator to metal transition and metal to insulator transition. (b) The optical conductivity of LSMO was obtained by ellipsometry. (c)The electronic structure schematic of LSMO films indicated the d-d transition, with the Fermi level represented by a red line.

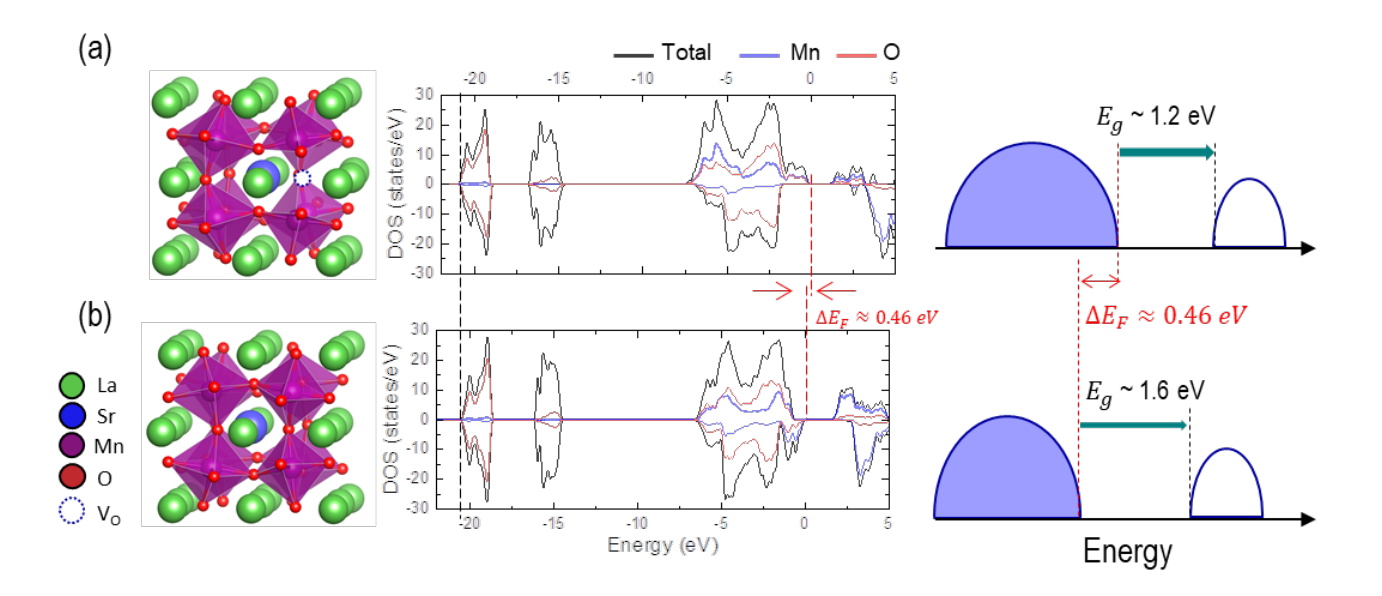


Figure 3. DFT optimized structures and projected density of states of (a) $La_{0.875}Sr_{0.125}MnO_3$ with V_O and (b) $La_{0.875}Sr_{0.125}MnO_3$. We aligned the O 1s level of the $La_{0.875}Sr_{0.125}MnO_3$ structure with the O 1s level of $La_{0.875}Sr_{0.125}MnO_3$ with V_O structure on the same line (black dashed line) to compare the Fermi levels of two structures. Zero energy represents the Fermi level. Schematic DOS near Fermi level for $La_{0.875}Sr_{0.125}MnO_3$ with V_O and $La_{0.875}Sr_{0.125}MnO_3$ show the energy difference between two fermi level, and band gap.

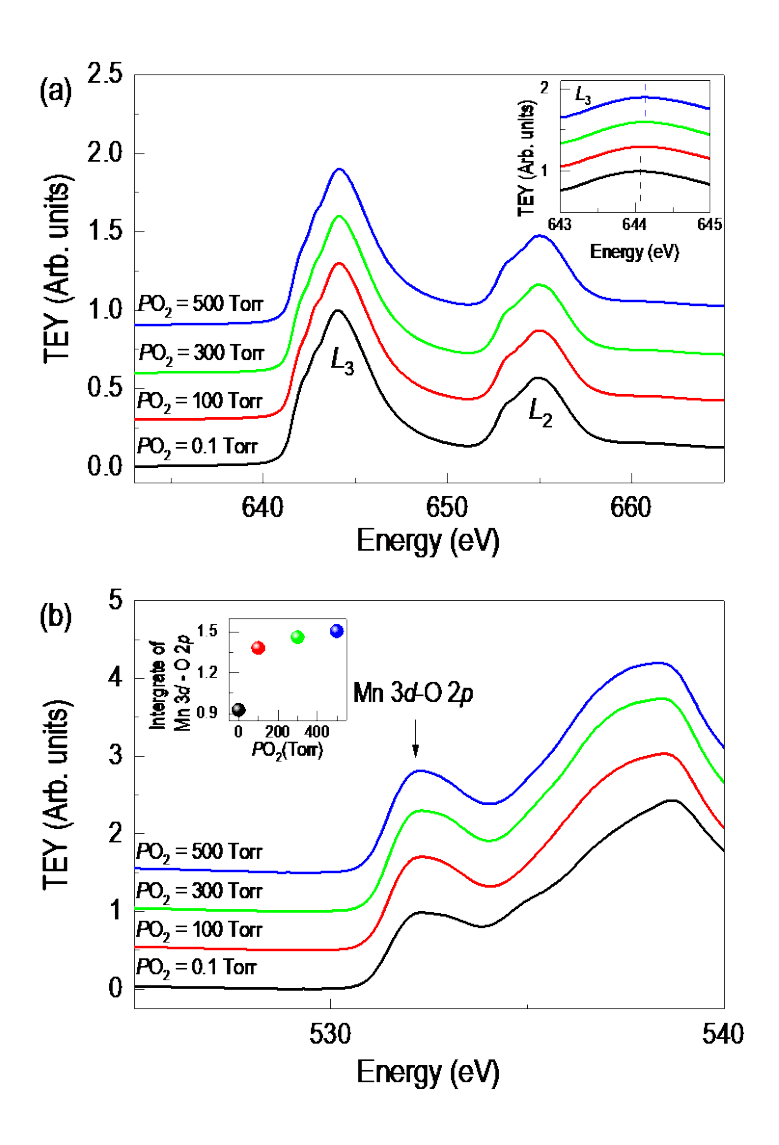


Figure 4. (a) The Mn L-edge spectra and (b) O K-edge spectra of LSMO thin films were obtained through x-ray absorption spectroscopy at room temperature. (inset in (a)) The peak of the Mn L_3 -edge shifts to higher energy with an increase in cooling PO_2 . (Inset in (b)) The integrated value of the peak of Mn 3d-O 2p hybridization peak intensity of LSMO films cooled at higher PO_2 shifts to a higher value.